Scientific Research Publishing

Open Journal of Physical Chemistry, 2026, 16(3), 59-76
https://www.scirp.org/journal/ojpc
ISSN Online: 2162-1977
ISSN Print: 2162-1969

Mussaenda erythrophylla Extracts as Green Corrosion Inhibitors for Aluminum Alloy in HCl: An Integrated Experimental and DFT Study

Aphouet A. Koffi[1*], Srinivasan Muralidharan[2], Paulin M. Niamien[1], Albert Trokourey[1]

[1]Laboratoire de Constitution et Réaction de la Matière, Université Félix Houphouët Boigny, Abidjan, Côte d'Ivoire
[2]Corrosion and Materials Protection Division, CSIR-Central Electrochemical Research Institute, Karaikudi, India
Email: *aphouet.koffi32@ufhb.edu.ci, koffiaphouet@yahoo.fr

How to cite this paper: Koffi, A.A., Muralidharan, S., Niamien, P.M. and Trokourey, A. (2026) *Mussaenda erythrophylla* Extracts as Green Corrosion Inhibitors for Aluminum Alloy in HCl: An Integrated Experimental and DFT Study. *Open Journal of Physical Chemistry*, **16**, 59-76.
https://doi.org/10.4236/ojpc.2026.163005

Received: June 1, 2026
Accepted: August 28, 2026
Published: August 31, 2026

Abstract

In alignment with green chemistry principles, this study evaluates the corrosion inhibition performance of leaf (MELE) and flower (MEFE) extracts of *Mussaenda erythrophylla* on silicon-aluminum alloy in 0.5 M HCl. A multidimensional approach integrating gravimetric and electrochemical techniques, gas chromatography-mass spectrometry (GC-MS), scanning electron microscopy (SEM), and density functional theory (DFT) at the B3LYP/6-311G level was employed to investigate both the macroscopic inhibition behavior and the underlying molecular mechanisms. Both extracts significantly mitigated aluminum alloy corrosion in the aggressive acidic medium, achieving inhibition efficiencies of 86.78% (MELE) and 84.75% (MEFE) at 0.35 g·L^{-1}. Inhibition was governed by adsorption onto anodic and cathodic sites, consistent with the Langmuir modified adsorption isotherm. SEM analysis revealed a marked reduction in pitting corrosion, confirming the protective role of the adsorbed organic film. GC-MS profiling identified the predominant constituents in each extract: di-n-octyl phthalate and 4,8,12-tetradecatrien-1-ol, 5,9,13-trimethyl in MELE, and phenol, 2,6-bis(1,1-dimethylethyl) in MEFE. Global reactivity descriptors (E_{HOMO}, E_{LUMO}, ΔE, electronegativity χ, hardness η, softness σ, electrophilicity index ω, and fraction of electrons transferred ΔN) revealed strong electron-donating and electron-accepting capacities, along with favorable adsorption energetics.

Keywords

Mussaenda erythrophylla, Green Corrosion Inhibitor, Electrochemical Measurements, Gravimetric Analysis, Density Functional Theory

1. Introduction

Aluminum and its alloys are indispensable materials across numerous industries, from aerospace to household goods, owing to their favorable strength-to-weight ratio and manufacturability [1]. However, a significant challenge arises during industrial cleaning processes. Acidic solutions, particularly hydrochloric acid used in metal pickling baths, are essential for descaling and cleaning installations, but aggressively attack aluminum [2]. Although aluminum naturally forms a protective oxide layer, this passivating film becomes unstable in acidic media, leading to corrosive dissolution.

To mitigate this degradation, the use of corrosion inhibitors is crucial. These compounds adsorb onto the metal surface at low concentrations, forming a protective barrier that significantly reduces dissolution. The adsorption mechanism typically involves either physical interaction (charge transfer with the charged metal surface) or chemical bonding (electron donation to the metal's vacant d-orbitals) [3] [4].

Despite their efficacy, many conventional synthetic inhibitors are toxic and raise environmental concerns, motivating a search for sustainable alternatives. This has catalysed significant research into plant-based extracts as viable, eco-friendly corrosion inhibitors [5]-[9]. Their appeal lies in a compelling combination of biodegradability, low toxicity, cost-effectiveness, and renewable abundance [6]. The versatility of this green approach is well documented, with extracts from a diverse range of botanical sources, including leaves [10]-[17], flowers [18], seeds [19], roots [20], stems [21], and fruit peels [22], demonstrating notable efficacy.

The inhibitory action of these extracts is attributed to bioactive phytochemicals, including tannins, flavonoids, and alkaloids. These molecules, often rich in heteroatoms (N, O, S) and π-electron systems, readily adsorb onto metal surfaces to form a protective film. The specific composition and concentration of these active compounds, and thus the extract's effectiveness, are highly dependent on the plant organ selected for extraction.

Guided by this rationale, the present study investigates the corrosion inhibition potential of *Mussaenda erythrophylla* leaf and flower extracts on a silicon-aluminum alloy in an acidic medium, using a combined experimental and theoretical approach. The experimental investigation employs gravimetric and electrochemical techniques to quantitatively evaluate the inhibitor's performance. These empirical findings are complemented by density functional theory (DFT) calculations and thermodynamic analyses to elucidate the fundamental adsorption mechanisms and active sites responsible for the protective effect.

2. Materials and Methods

2.1. Materials and Test Solutions

The study utilized a rectangular silicon-aluminum alloy coupon (2 cm × 4 cm × 0.05 cm) with the following chemical composition (wt.%): 2.23% Si, 0.57% Fe,

0.1% Cr, 0.07% Cu, 0.03% Ti, 0.02% Zn, 0.02% Pb, and the balance aluminum, as determined at the CSIR-Central Electrochemical Research Institute (CSIR-CECRI), India.

The aggressive medium was a 0.5 M HCl solution, prepared by diluting a commercial 35 % analytical-grade reagent (RANKEM) with bidistilled water. Inhibitor solutions containing MELE and MEFE plant extracts were tested at concentrations between 0.1 and 0.35 $g{\cdot}L^{-1}$. To prepare the two extracts, leaves and flowers of *Mussaenda erythrophylla*, a species commonly cultivated in Indian gardens and parks, were collected from CSIR-CECRI. The fresh plant material was rinsed, shade-dried at ambient temperature, and ground to a homogeneous powder (200 g). Soxhlet extraction of the powdered material was conducted with an ethanol-water mixture (80:20, v/v) using a 500 mL Borosil apparatus; the process was deemed complete when the solvent in the siphon tube appeared colourless. The crude extract was concentrated to roughly 100 mL, defatted with petroleum ether, and the alcoholic phase was separated, further concentrated to approximately 50 mL, and dried in a vacuum oven at 60˚C for three days. The resultant dark brown solid (30 g) was kept in a desiccator until required. All solvents were freshly distilled before use, and all experiments were performed using glass vessels to minimize the risk of contamination from plastic materials.

2.2. Corrosion Assessment by Mass Loss

Corrosion inhibition was evaluated using the mass loss technique, a widely adopted method due to its simplicity and reliability [23] [24]. Before testing, the specimens were progressively abraded with emery paper to achieve a mirror-like finish, followed by rinsing with distilled water, degreasing with acetone, and air-drying. Triplicate samples were accurately weighed before being immersed in the hydrochloric acid solution using a glass hook, both in the absence and presence of the extracts. The temperature was maintained between 25˚C and 45˚C using a thermostatically controlled bath. After a 1-hour immersion period, the three specimens were retrieved, thoroughly cleaned, dried, and weighed again. The corrosion rate (CR) was then determined according to the following relationship:

$$\mathrm{CR} = \frac{m_1 - m_2}{St}. \tag{1}$$

where m_1 and m_2 are the mass (in g) before and after immersion in the test solution, respectively, S is the total surface of the sample (in cm^2), and t is the immersion time (in h). The inhibition efficiency IE (%) was then calculated using the following relation:

$$\mathrm{IE}(\%) = \frac{w_0 - w}{w_0} \times 100. \tag{2}$$

In this equation, w_0 and w are the corrosion rates of the aluminium in the absence and presence of the investigated extract, respectively.

2.3. Potentiodynamic Polarization and EIS Measurements

Potentiodynamic polarization and electrochemical impedance spectroscopy (EIS) were conducted using a standard three-electrode cell setup. The electrochemical cell consisted of a platinum foil (1 cm^2) as the counter electrode (CE), a saturated calomel electrode (SCE) as the reference electrode, and a silicon-aluminum alloy sample as the working electrode (WE). The aluminum samples were embedded in epoxy resin, exposing only a 1 cm^2 surface area. The exposed surface was prepared following the procedure outlined in the previous section. All experiments were performed using a Gill AC Model 1566 electrochemical instrument. Before measurements, the open-circuit potential (OCP) was established by monitoring the potential over time, both to verify attainment of a steady state and to determine the necessary immersion time for stabilization. Polarization curves were then recorded within a range of −200 mV to +200 mV relative to the OCP, with a scan rate of 1 mV/s. EIS measurements were carried out across a frequency range of 100 kHz to 100 mHz, with an AC amplitude of 10 mV. Each electrochemical experiment was repeated at least three times at room temperature to check the reproducibility in aerated condition.

2.4. Gas Chromatography-Mass Spectroscopy (GC-MS) Characterization

The volatile compounds in the plant extracts (MELE and MEFE) were analyzed by gas chromatography-mass spectrometry (GC-MS). For analysis, 10 mg of each extract was dissolved in 10 mL of ethanol. The resulting solution was filtered, centrifuged at 10,000 rpm for 20 minutes, and filtered again. A 1 µL aliquot of the purified solution was injected into the GC-MS system. The analysis was performed using an Agilent Technologies 5975C Inert MSD with a Triple-Axis detector. Separation was achieved on a DB-5 fused silica capillary column (30 m × 0.25 mm ID × 0.25 µm film thickness) with helium as the carrier gas at a constant flow rate of 1.0 mL/min. The injector temperature was set to 275˚C, and samples were injected in split mode with a 10:1 ratio.

The oven temperature program was as follows: initial hold at 110˚C for 2 minutes, ramped to 200˚C at 10˚C/min, held at 200˚C for 9 minutes, then ramped to 280˚C at 5˚C/min, with a final hold at 280˚C for 2 minutes. The mass spectrometer transfer line was maintained at 280˚C. Electron ionization (EI) at 70 eV was used, and mass spectra were acquired in scan mode over a mass range of 20 - 600 *m/z* with a scan rate of 0.5 seconds per scan. Compound identification was conducted by comparing the acquired mass spectra against those in the National Institute of Standards and Technology (NIST) mass spectral library.

2.5. Surface Morphology Analysis by Scanning Electron Microscopy (SEM)

The surface morphology of the silicon-aluminum alloy samples after immersion in the test solutions was characterized by scanning electron microscopy (SEM)

using a TESCAN microscope. Micrographs were acquired at 1000× magnification using the secondary electron detector, with an accelerating voltage of 15 kV, a working distance of 17 mm, and a 127 µm aperture.

2.6. Density Functional Theory (DFT) Calculations

The molecular properties of the extract's main constituents were determined using density functional theory (DFT). Initial molecular structures were constructed and pre-optimized using GaussView 6.0.16. Subsequent quantum chemical calculations were performed using Gaussian 09 W software without imposing symmetry constraints. The B3LYP hybrid functional (Becke's three-parameter exchange with Lee-Yang-Parr correlation) [25] [26] was employed with the 6 - 311 G basis set for all computations [27].

3. Results and Discussion

3.1. Gravimetric Assessment of Corrosion Behavior

The corrosion rate of aluminium in 0.5 M HCl was evaluated using mass loss data, both with and without plant extracts (MELE and MEFE). As shown in **Figure 1**, the corrosion rate at 25˚C decreases significantly with the addition of the extracts and exhibits a concentration-dependent decline. This trend confirms that both MELE and MEFE act as effective corrosion inhibitors for aluminium in acidic media.

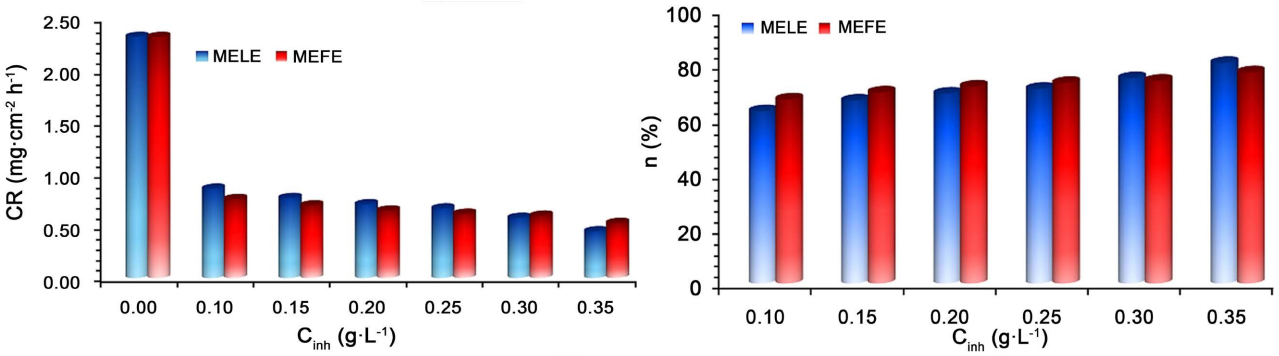

Figure 1. (a) Corrosion rate and (b) Inhibition efficiency with increasing concentration of *Mussaenda erythrophylla* extracts (MELE and MEFE) for silicon-aluminum alloy immersed in 0.5 M HCl at 25˚C.

The inhibition efficiency (**Figure 1**) increases with inhibitor concentration for both extracts, reaching values between 60% and 85% as the concentration rises from 0.1 g·L^{-1} to 0.35 g·L^{-1}. This trend suggests enhanced surface coverage due to greater inhibitor adsorption on the metal surface [3] [8]. Despite their different chemical compositions, MELE and MEFE exhibit comparable performance, a similarity that can be traced to their shared functional features, namely aromatic rings, extended carbon chains, and oxygenated moieties, which govern their adsorption behavior on the metal surface.

3.2. Study on the Adsorption Behavior and Isotherm Modeling

The inhibitory effectiveness of an organic compound is primarily determined by its ability to adsorb onto the substrate, forming a protective layer. The adsorption process is commonly described as a substitution reaction where inhibitor molecules in the aqueous solution, $\mathrm{In}h_{(sol)}$, displace water molecules, $\mathrm{H_2O}_{(ads)}$ previously adsorbed on the metal surface [28]:

$$x\mathrm{H_2O}_{(ads)} + \ln h_{(sol)} \rightleftarrows \ln \mathrm{h}_{(ads)} + x\mathrm{H_2O}_{(sol)} . \tag{3}$$

In this equation, x corresponds to the number of water molecules replaced by a single inhibitor molecule. To analyze the adsorption behavior of the extracted inhibitors on the aluminum alloy surface, several adsorption isotherm models were applied to fit the experimental data. Among the models tested, the Langmuir adsorption isotherm provided the best correlation. The standard Langmuir isotherm is expressed as follows, where K_{ads} represents the equilibrium constant for the adsorption process.

$$\frac{C_{inh}}{\theta} = \frac{1}{K_{ads}} + C_{inh} . \tag{4}$$

However, the Langmuir plot exhibited a slope deviating from unity (**Table 1**), indicating deviations from ideal monolayer adsorption behavior. This suggests phenomena such as multilayer formation or repulsive interactions between adsorbed molecules [24] [29]. The adsorption equilibrium constant (K_{ads}) was subsequently determined using the modified Langmuir isotherm proposed by Villamil *et al.*, as shown in Equation (5).

$$\frac{C_{inh}}{\theta} = \frac{n}{K_{ads}} + nC_{inh} . \tag{5}$$

Table 1. Parameters derived from the straight line of the Langmuir isotherm.

Plant extract	Equation	Coefficient determination	K_{ads} (L·g^{-1})	ΔG_{ads} (k·Jmol^{-1})
MELE	y = 1.1236x + 0.0567	0.9887	19.82	−24.93
MEFE	y = 1.2328x + 0.0294	0.9983	41.93	−26.81

The standard Gibbs free energy of adsorption (ΔG_{ads}) is deduced from the following expression:

$$\Delta G_{ads} = -RT \ln\left(C_e K_{ads}\right) \tag{6}$$

where R is the universal gas constant, T is the absolute temperature, and C_e is the concentration of water, taken as 1000 g·L^{-1} (55.5 mol·L^{-1}). The calculated ΔG_{ads} value is negative, confirming the spontaneity of the adsorption process. According to established literature [24] [29] [30], the magnitude of ΔG_{ads} provides insight into the adsorption mechanism. Values lower than −40 kJ·mol^{-1} involve charge sharing; those higher than −20 kJ·mol^{-1} are consistent with electro-

static interaction; and those between these two values indicate both physisorption and chemisorption. Based on this framework, the calculated value close to −20 kJ·mol^{-1} could express the predominance of physisorption.

3.3. Effect of Temperature on the Corrosion Inhibition of Silicon-Aluminum Alloy in HCl Medium

To elucidate the mode of adsorption, the corrosion rate of the silicon-aluminum alloy in 0.5 M HCl was investigated as a function of temperature (25˚C - 45˚C), both in the absence and presence of the plant extracts (0.35 g·L^{-1}). The apparent activation energy (E_a) was determined from the Arrhenius plot (Equation (7)), while the enthalpy (ΔH_a^*) and entropy (ΔS_a^*) of activation were calculated from the transition state plot (Equation (8)) [31] [32]. The linearity of the plots ($R^2 > 0.9$) confirms the applicability of these models. The calculated thermodynamic parameters are summarized in Table 2.

$$\log CR = \log A - \frac{E_a}{2.303RT}. \tag{7}$$

$$\log\left(\frac{CR}{T}\right) = \left[\log\left(\frac{R}{\aleph h}\right) + \frac{\Delta S_a^*}{2.303R}\right] - \frac{\Delta H_a^*}{2.303RT}. \tag{8}$$

A key finding is the higher activation energy for the inhibited systems compared to the blank acid. This is a typical indicator of physisorption, where the inhibitor creates an additional energy barrier for the corrosion process [33]. The positive values of ΔH_a^* confirm the endothermic nature of the silicon-aluminum alloy dissolution, which is inherently energetically challenging [30]. The further increase in ΔH_a^* in the presence of the inhibitors reflects their enhanced protective efficiency. Furthermore, the increase in the entropy of activation (ΔS_a^*) suggests a more disordered state in the activated complex relative to the reactants. This is consistent with the desorption of water molecules upon inhibitor adsorption, leading to a net increase in the system's disorder, which also supports a physical adsorption mechanism [30] [34].

Table 2. Activation parameters for aluminium dissolution in 0.5 M HCl, without and with MELE and MEFE inhibitors across a temperature range of 25˚C to 45˚C.

0.5 M HCl	E_a kJ·mol^{-1}	ΔH_a^* kJ·mol^{-1}	ΔS_a^* kJ·mol^{-1}
Blank	89.90	87.30	447.68
MELE	91.25	88.65	437.52
MEFE	112.06	109.46	506.85

3.4. Electrochemical Approach

Electrochemical measurements of the plant extract's inhibitory properties have elucidated the mechanisms of the silicon-aluminum alloy corrosion and inhibitor adsorption. Figure 2 presents the open-circuit potential (OCP) plots and potentiodynamic polarization curves. In the blank acid solution, the OCP rose rapidly

during the first 1000 seconds as the protective Al_2O_3 layer dissolved, then continued to increase gradually before stabilizing after approximately 8100 seconds. In contrast, the inhibited solutions reached a steady state much earlier, at 4800 seconds, demonstrating the protective effect of the extracts. The Tafel curves, recorded after a fixed immersion time of 9000 seconds to ensure consistency, are also shown in **Figure 2**. The linear segment of the cathodic branch indicates that the hydrogen evolution reaction is controlled by a pure activation mechanism [35]. The unchanged shape of the curves in the inhibited solution implies that adding 0.35 g·L^{-1} of the plant extract does not alter the corrosion mechanism but significantly reduces the corrosion current density (i_{corr}). **Table 3** lists the parameters derived from the polarization curves. The observed shift in corrosion potential (E_{corr}) was less than ±85 mV, which is insufficient to classify the inhibitors as purely anodic or cathodic. According to the literature [2] [24], this indicates a mixed-type inhibitory behavior. The inhibitory efficiencies, calculated using Equation (9), corroborate the gravimetric results. In this relation, i_{corr} and $i_{corr(inh)}$ are the corrosion densities in blank and inhibited solutions, respectively.

$$IE_p(\%) = \frac{i_{corr} - i_{corr(inh)}}{i_{corr}} \times 100. \quad (9)$$

Table 3. Electrochemical parameters for silicon-aluminum alloy in 0.5 M HCl, without and with plant extracts.

	Open-circuit potential and Tafel parameters					
	E_{OCP} (mV)	E_{corr} (mV vs.SCE)	bc (mV/dec)	ba (mV/dec)	i_{corr} (mA/cm^2)	IE_p (%)
Blank	−742 ± 45	−746 ± 56	199.5 ± 6.9	70.41 ± 2.11	5.90 ± 0.23	
MELE	−753 ± 47	−751 ± 57	132.2 ± 5.3	10.39 ± 0.32	0.78 ± 0.02	86.8 ± 5.2
MEFE	−751 ± 38	−750 ± 46	136.1 ± 8.1	13.12 ± 0.46	0.90 ± 0.02	84.8 ± 5.1
	Nyquist plots parameters obtained from Re-Q|(RP-(L|Rind)) equivalent circuit					
	Q (CPE)					
	Re (Ω·cm^2)	Y0 (μS·s$^{\alpha}$·cm^{-2})	α	Rp (Ω·cm^2)	L (H·cm^2)	Rind (Ω·cm^2)	Rt (Ω·cm^2)	IEEIS (%)
Blank	2.57 ± 0.09	141 ± 13	0.84 ± 0.01	2.71 ± 0.20	2.64 ± 0.11	10.67 ± 0.18	13.38 ± 0.38	
MELE	2.28 ± 0.27	50 ± 2	0.89 ± 0.01	25.35 ± 1.06	41.85 ± 1.08	100.50 ± 1.07	125.85 ± 2.13	89.4 ± 2.3
MEFE	2.47 ± 0.24	57 ± 2	0.87 ± 0.01	16.38 ± 0.36	16.18 ± 0.36	70.26 ± 0.74	86.64 ± 1.10	84.6 ± 1.7

Electrochemical impedance spectroscopy (EIS) was performed over a frequency range of 100 kHz to 0.1 Hz. The resulting Nyquist plots (**Figure 2**) are characterized by a broad capacitive arc and a similarly sized inductive loop. The capacitive arc at high-to-intermediate frequencies represents the charge transfer process at the metal/electrolyte interface, associated with the dissolution of the silicon-aluminum alloy oxide layer and the formation of the electrochemical double layer [2] [17]. The addition of 0.35 g·L^{-1} of the plant extract significantly increased the diameter of this capacitive arc, confirming the inhibitory effect of MELE and MEFE. The protective barrier formed by adsorbed inhibitor molecules effectively shields

the aluminum alloy surface from corrosion. The inductive half-loop, a characteristic feature of aluminum in hydrochloric acid, is often attributed to the adsorption of species (e.g., H^+, Cl^- ions, or inhibitor molecules) [20] [36], their relaxation on the surface [37], or the redissolution of the passivated metal [38]. At low frequencies, the appearance of diffusion-related processes indicates that the adsorption is constrained by the diffusion of species from the solution. The overall similarity of the Nyquist spectra suggests that the corrosion mechanism is unchanged by the inhibitors [39]. However, the capacitive loops deviate from an ideal semicircle, a phenomenon known as frequency dispersion, which is attributed to the non-uniform distribution of reaction sites across the metal surface [40]. The corrosion processes are modeled by the equivalent circuit in **Figure 2**, where Re represents the electrolyte resistance. The double-layer capacitance is represented by a constant phase element (CPE) in parallel with the polarization resistance (Rp), which characterizes the charge transfer resistance. The inductive behavior is modeled by an inductance (L) in series with an inductive resistance (Rind). The electrochemical parameters obtained from fitting the experimental data to this circuit are summarized in **Table 3**.

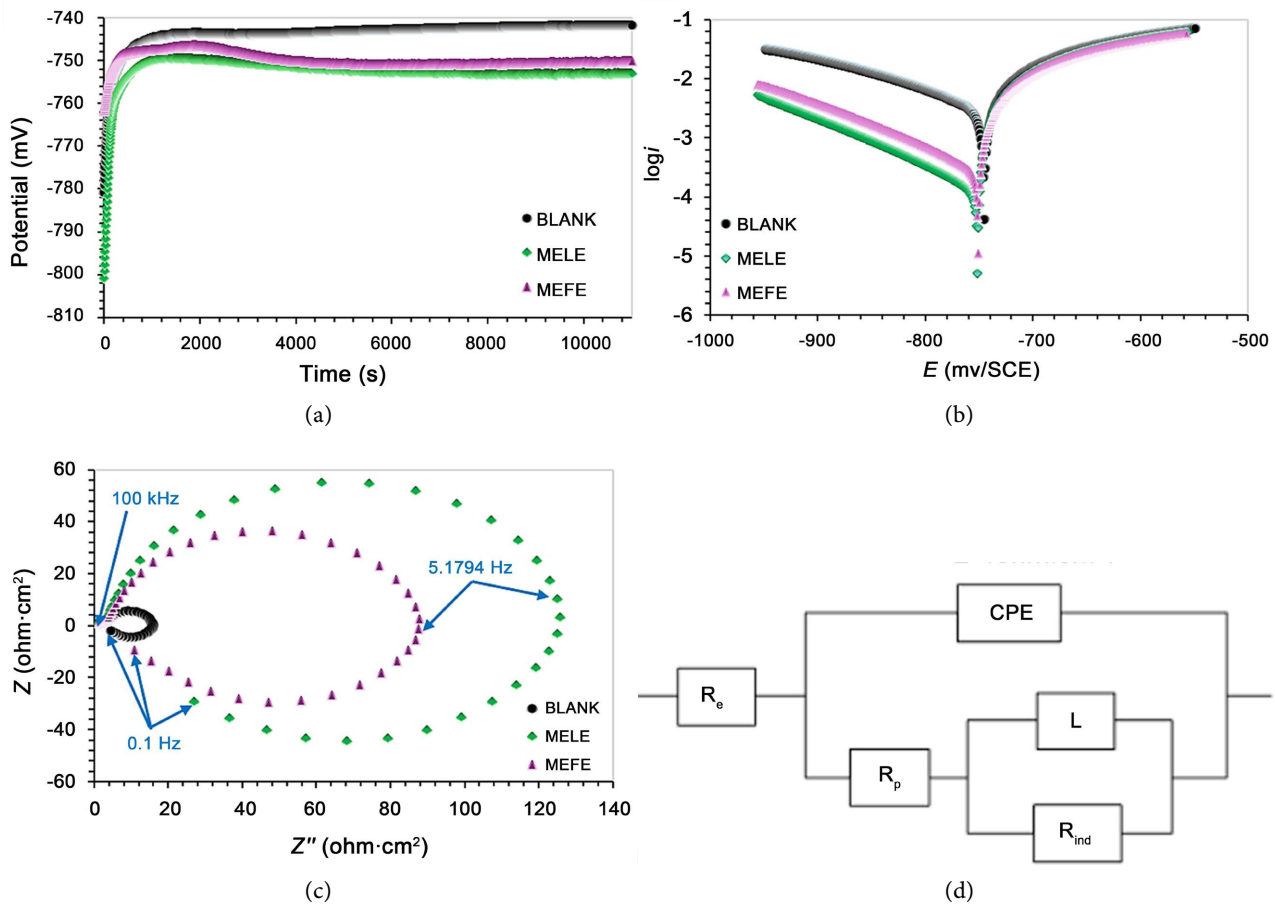

Figure 2. (a) Open-circuit potential (OCP) and (b) potentiodynamic polarization (Tafel) curves for a silicon-aluminum alloy in 0.5 M HCl solution in the absence and presence of plant extract inhibitors; (c) Nyquist diagrams and (d) corresponding equivalent circuit models for the blank and extract-containing solutions.

3.5. SEM Analysis of Silicon-Aluminum Alloy Surface Morphology

The surface analysis by the SEM tool is shown in Figure 3. The aluminum alloy was deeply corroded after its contact with the blank acid solution at 25˚C. This is pitting corrosion over virtually the entire surface of the substrate. However, the corrosion attack was significantly reduced by adding 0.35 $g{\cdot}L^{-1}$ of plant extracts. The attack was limited in some areas of the metal, and certain regions remained unaffected by the aggressive environment.

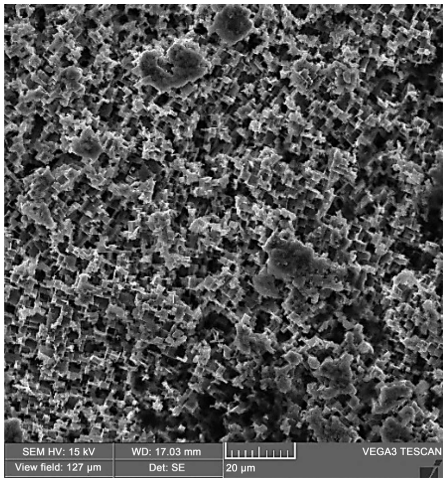

(a)

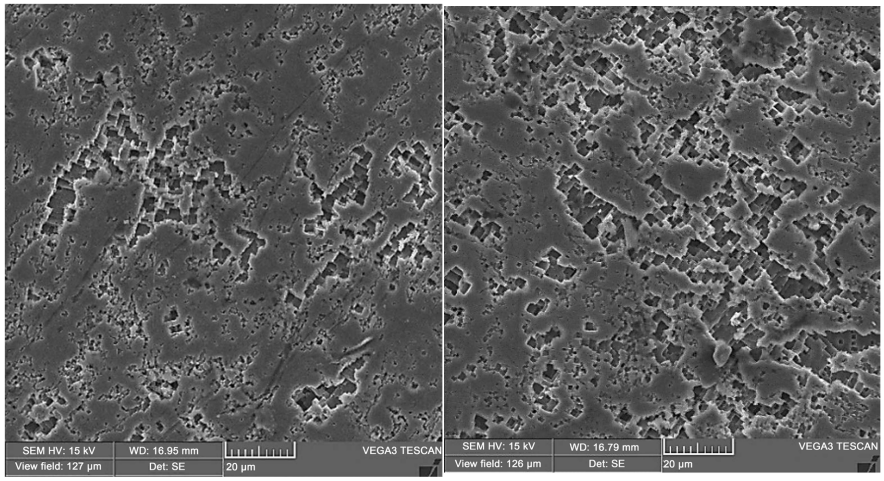

(b) (c)

Figure 3. SEM micrographs of the silicon-aluminum alloy surface after immersion in 0.5 M HCl solutions without and with *Mussaenda erythrophylla* extract. (a) Blank (b) Leaf Extract (c) Flower extract.

3.6. GC-MS Analysis

GC-MS analysis, referenced against the NIST database, identified a series of organic compounds bearing O-H, C=O, and C-O functional groups in the leaf (MELE) and flower (MEFE) extracts of *Mussaenda erythrophylla* (Table 4). The leaf extract (MELE) was found to be primarily composed of di-n-octyl phthalate

($C_{24}H_{38}O_4$) and 4,8,12-tetradecatrien-1-ol, 5,9,13-trimethyl ($C_{17}H_{30}O$) (Figure 4). In contrast, the dominant constituent in the flower extract (MEFE) was phenol, 2,6-bis(1,1-dimethylethyl) ($C_{14}H_{22}O$).

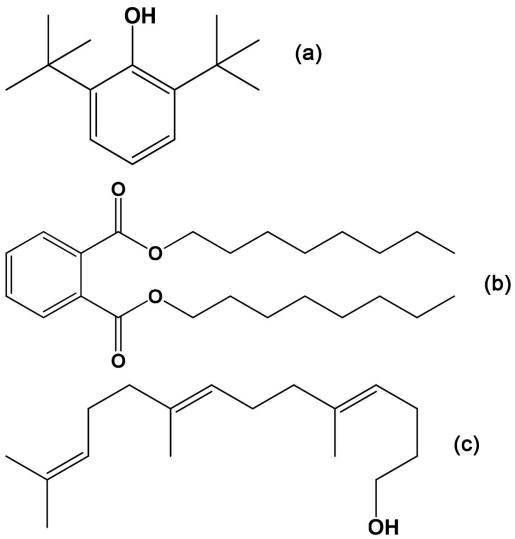

Figure 4. Major phytochemical constituents identified in the leaf (MELE) and flower (MEFE) extracts of *Mussaenda erythrophylla*. (a) phenol, 2,6-bis(1,1-dimethylethyl); (b) 4,8,12-tetradecatrien-1-ol, 5,9,13-trimethyl; (c) di-n-octyl phthalate.

Table 4. Chemical constituents identified by GC-MS analysis in the leaf (MELE) and flower (MEFE) extracts of *Mussaenda erythrophylla*. Compound identifications are based on the NIST Mass Spectral Database.

Retention time (min)	Compound	Molecular formula	Molecular weight ($g \cdot mol^{-1}$)
Mussaenda erythrophylla leaf extract (MELE)			
20.624	n-hexadecanoic acid	$C_{16}H_{32}O_2$	252
20.715	1,2-benzenedicarboxylic acid, monobutyl ester	$C_{12}H_{14}O_4$	222
24.304	octadecanoic acid, 2-(2 hydroxyethoxy) ethyl ester	$C_{22}H_{44}O_4$	372
30.648	di-n-octyl phthalate	$C_{24}H_{38}O_4$	390
34.690	4,8,12-tetradecatrien-1-ol, 5,9,13-trimethyl	$C_{17}H_{30}O$	250
Mussaenda erythrophylla flower extract (MEFE)			
10.260	dodecane	$C_{12}H_{26}$	170
13.534	tetradecane	$C_{14}H_{30}$	198
15.466	phenol, 2,6-bis(1,1-dimethylethyl)	$C_{14}H_{22}O$	206
20.471	phthalic acid, butyl tetradecyl ester	$C_{26}H_{42}O_4$	418
21.683	dibutyl phthalate	$C_{16}H_{22}O_4$	278
23.139	docosane, 11-butyl	$C_{26}H_{54}$	366

3.7. Analysis Using the DFT Approach

Density Functional Theory (DFT) has emerged in recent years as a critical computational tool for probing the molecular-level mechanisms of organic corrosion

inhibitors [41]-[43]. In this study, we applied DFT to evaluate three main metabolites from *Mussaenda erythrophylla*, di-n-octyl phthalate, 4,8,12-tetradecatrien-1-ol, 5,9,13-trimethyl, and phenol, 2,6-bis(1,1-dimethylethyl), by calculating their global chemical reactivity descriptors. A comparative analysis of their frontier molecular orbitals (HOMO and LUMO) reveals distinct electronic distributions across the three compounds, as illustrated in **Figure 5** and summarized in **Table 5**.

For di-n-octyl phthalate, the HOMO and LUMO are both centered on the phthalate core but differ in reactivity. The LUMO is strongly delocalized over the aromatic ring, with significant electron density on its carbon and oxygen atoms, identifying this region as the primary electrophilic site. In contrast, the HOMO, indicative of nucleophilic character, is also associated with the phthalate group but exhibits notably weaker density on the oxygen atoms. In phenol, 2,6-bis(1,1-dimethylethyl), the HOMO and LUMO show remarkably similar spatial distributions. Electrophilic density localizes on specific carbons of the benzene ring and methyl groups, whereas nucleophilic character is broadly delocalized throughout the phenolic system. The most extensive delocalization occurs in 4,8,12-tetradecatrien-1-ol, 5,9,13-trimethyl, where frontier orbitals spread across the conjugated carbon backbone. This distribution is non-uniform, with heightened electron density on methyl-substituted and terminal carbon atoms.

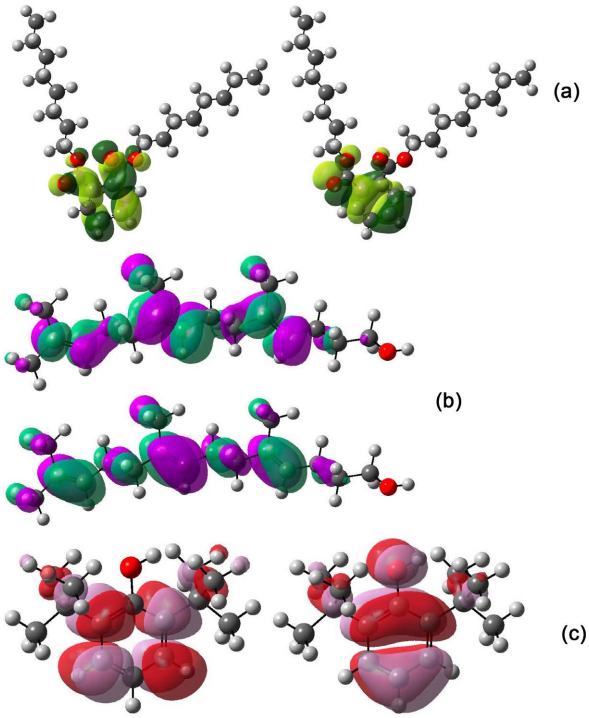

Figure 5. Frontier molecular orbitals (HOMO and LUMO) for the major compounds identified in the leaf (MELE) and flower (MEFE) extracts of *Mussaenda erythrophylla*. (a) LUMO (left) and HOMO (right) orbitals of di-n-octyl phthalate; (b) LUMO (left) and HOMO (right) orbitals of 4,8,12-tetradecatrien-1-ol, 5,9,13-trimethyl; (c) LUMO (left) and HOMO (right) orbitals of phenol, 2,6-bis(1,1-dimethylethyl).

Table 5 presents the calculated quantum chemical descriptors for these molecules. The LUMO energy, which reflects electron-accepting ability, is notably low for the two aromatic compounds, consistent with their high electron affinity. In contrast, HOMO energies, which indicate electron-donating tendency, are similar across all three, suggesting each can donate electrons to vacant metal orbitals [25] [44]. The energy gap, ΔE (Equation (10)), a key indicator of reactivity, aligns with literature values and supports the corrosion inhibition potential of these molecules [43] [45]. Additional global reactivity descriptors, including electronegativity (χ, Equation (11)), further elucidate the inhibitor-metal interaction [41].

$$\Delta E = E_{LUMO} - E_{HOMO}. \tag{10}$$

Table 5. Global reactivity descriptors of the leaf (MELE) and flower (MEFE) extracts of *Mussaenda erythrophylla* by DFT calculation.

Molecule	ELUMO (eV)	EHOMO (eV)	ΔE (eV)	χ (eV)	η (eV)	σ (eV)$^{-1}$	ω (eV)	ΔN
di-n-octyl phthalate	−1.860	−7.252	5.392	4.556	2.696	0.371	3.850	−0.051
4,8,12-tetradecatrien-1-ol, 5,9,13-trimethyl	0.378	−6.270	6.648	2.946	3.324	0.301	1.306	0.201
phenol, 2,6-bis(1,1-dimethylethyl)	−0.208	−6.232	6.024	3.220	3.012	0.332	1.721	0.176

Di-n-octyl phthalate exhibits a higher electronegativity, whereas the other two compounds have lower electronegativities relative to the work function of aluminium (Φ_{Al} = 4.28 eV) [46]. This difference leads to distinct electron-transfer behaviors, quantified by the fraction of transferred electrons, ΔN (Equation (12)).

$$x = \frac{1}{2}\left(E_{LUMO} + E_{HOMO}\right). \tag{11}$$

$$\Delta N = \frac{\Phi_{Al} - x_{inh}}{2\left(\eta_{Al} + \eta_{inh}\right)}. \tag{12}$$

Here, Φ_{Al} = 4.28 eV and η_{Al} = 0 for aluminum [30] [46]. A positive ΔN (>0) implies electron donation from inhibitor to metal, observed for the 4,8,12-tetradecatrien-1-ol, 5,9,13-trimethyl and the phenolic compound. Conversely, the negative ΔN (<0) for di-n-octyl phthalate suggests electron back-donation from the metal to the inhibitor. The electrophilicity index (ω) measures stabilization energy upon electron acquisition [43]. The di-n-octyl phthalate acts as the strongest electrophile (ω = 3.850 eV), while the aliphatic alcohol behaves as a moderate electrophile (ω = 1.306 eV). Finally, hardness (η; Equation (14)) and softness (σ; Equation (15)) provide insight into molecular reactivity [45]. The aromatic compounds are softer (lower η), indicating greater reactivity than the harder tetradecatrienol.

$$\omega = \frac{\left(\mu\right)^2}{2 \times x}. \tag{13}$$

$$\eta = \frac{E_{LUMO} - E_{HOMO}}{2}. \tag{14}$$

$$\sigma = \frac{1}{\eta}. \tag{15}$$

In summary, the combination of a low ΔE gap, complementary electron-transfer mechanisms (ΔN), strong electrophilicity, and favorable softness values demonstrates that all three molecules can participate effectively in forming a protective barrier on the silicon-aluminum alloy surface through synergistic interactions with the metal substrate.

4. Conclusion

This combined experimental and computational study demonstrated the corrosion inhibition potential of *Mussaenda erythrophylla* extracts on a silicon-aluminum alloy in 0.5 M HCl. Gravimetric and electrochemical measurements converged to confirm the effectiveness of both leaf (MELE) and flower (MEFE) extracts, achieving inhibition efficiencies of 86.78% and 84.75%, respectively, at 0.35 $g{\cdot}L^{-1}$ without altering the underlying reaction mechanism. Inhibition proceeds via the adsorption of organic constituents onto the metal surface, as evidenced by electrochemical impedance spectroscopy and electron microscopy, the latter revealing a marked suppression of pitting corrosion. GC-MS analysis identified the predominant bioactive constituents, di-n-octyl phthalate and 4,8,12-tetradecatrien-1-ol, 5,9,13-trimethyl in MELE, and a disubstituted phenol in MEFE, and subsequent DFT evaluation of their electronic properties established clear correlations between molecular reactivity and the measured inhibition performance. Collectively, these findings support an adsorption-mediated inhibition mechanism and highlight the promising potential of plant-derived extracts as effective, environmentally benign corrosion inhibitors.

Acknowledgements

Aphouet A. Koffi expresses gratitude to the Council of Scientific and Industrial Research (CSIR), India, and The World Academy of Sciences (TWAS), Italy, for granting the PG Research Fellowship (Letter dated 05/03/2013, FR number: 3240267285). The authors also extend their appreciation to the CSIR-CECRI, Karaikudi, India, for its valuable support and keen interest in this work.

Author Contributions

Conceptualization, A.A.K. and A.T.; methodology, A.A.K.; software, S.M. and P.M.N.; validation, A.A.K., S.M. and A.T.; formal analysis, A.A.K. and P.M.N.; investigation, A.A.K.; resources, A.A.K. and S.M.; data curation, P.M.N. and A.T.; writing—original draft preparation, A.A.K.; writing—review and editing, A.A.K.; visualization, A.A.K.; supervision, A.T.; project administration, S.M.; funding acquisition, A.A.K. and S.M. All authors have read and agreed to the published version of the manuscript.

Conflicts of Interest

This manuscript is the authors' original work, has not been previously published

or copyrighted, and is not under consideration elsewhere. It will not be submitted to another journal while under review by Open Journal of Physical Chemistry. The authors declare no conflicts of interest, have approved the submission, and meet the authorship criteria established by Open Journal of Physical Chemistry.

References

[1] Gummanar, N., Mokshanatha, P.B., Dyapur, P. and Yallappa, G.N. (2023) Organic Corrosion Inhibitors for Aluminum-Based Alloys—A Review. *Letters in Applied NanoBioScience*, **12**, Article 170.

[2] Raviprabha, K., Bhat, R.S., Bhat, S.I., Nagaraj, P. and Jyothi, K. (2023) Corrosion Inhibition Study of 6061 Aluminium Alloy in the Presence of Ethyl 5-Methyl-1-(4-Nitrophenyl)-1H-1,2,3-Triazole-4-Carboxylate (NTE) in Hydrochloric Acid. *Heliyon*, **9**, e16036. https://doi.org/10.1016/j.heliyon.2023.e16036

[3] Shwetha, K.M., Praveen, B.M. and Devendra, B.K. (2024) A Review on Corrosion Inhibitors: Types, Mechanisms, Electrochemical Analysis, Corrosion Rate and Efficiency of Corrosion Inhibitors on Mild Steel in an Acidic Environment. *Results in Surfaces and Interfaces*, **16**, Article 100258. https://doi.org/10.1016/j.rsurfi.2024.100258

[4] Fouda, A.S., Abdel-Wahed, H.M., Atia, M.F. and El-Hossiany, A. (2023) Novel Porphyrin Derivatives as Corrosion Inhibitors for Stainless Steel 304 in Acidic Environment: Synthesis, Electrochemical and Quantum Calculation Studies. *Scientific Reports*, **13**, Article No. 17593. https://doi.org/10.1038/s41598-023-44873-2

[5] Ahmed, M.A., Amin, S. and Mohamed, A.A. (2024) Current and Emerging Trends of Inorganic, Organic and Eco-Friendly Corrosion Inhibitors. *RSC Advances*, **14**, 31877-31920. https://doi.org/10.1039/d4ra05662k

[6] Baari, M.J. and Sabandar, C.W. (2021) A Review on Expired Drug-Based Corrosion Inhibitors: Chemical Composition, Structural Effects, Inhibition Mechanism, Current Challenges, and Future Prospects. *Indonesian Journal of Chemistry*, **21**, 1316-1336. https://doi.org/10.22146/ijc.64048

[7] Vaszilcsin, N., Kellenberger, A., Dan, M.L., Duca, D.A. and Ordodi, V.L. (2023) Efficiency of Expired Drugs Used as Corrosion Inhibitors: A Review. *Materials*, **16**, Article 5555. https://doi.org/10.3390/ma16165555

[8] Holla, B.R., Mahesh, R., Manjunath, H.R. and Anjanapura, V.R. (2024) Plant Extracts as Green Corrosion Inhibitors for Different Kinds of Steel: A Review. *Heliyon*, **10**, e33748. https://doi.org/10.1016/j.heliyon.2024.e33748

[9] Thacker, H. and Ram, V. (2025) Green Corrosion Inhibitors Derived from Plant Extracts and Drugs for Mild Steel in Acid Media: A Review. *Results in Surfaces and Interfaces*, **18**, Article 100364. https://doi.org/10.1016/j.rsurfi.2024.100364

[10] Oguike, R.S., Oni, O., Barambu, A.U., Balarak, D., Buba, T., Okeke, C.U., *et al.* (2021) Computational Stimulation and Experimental Study on Corrosion Inhibition Qualities of *Emilia sonchifolia* Leaf Extract for Copper (CU131729) in Hydrochloric Acid. *Computational Chemistry*, **9**, 18-36. https://doi.org/10.4236/cc.2021.91002

[11] Hatem, O.A. (2022) Computational and Experimental Evaluation of Inhibition Potential of a New Ecologically Friendly Inhibitor Leaves of Date Palm (*Phoenix dactylifera* L.) for Aluminium Corrosion in an Acidic Media. *International Journal of Corrosion*, **2022**, Article ID: 5953561. https://doi.org/10.1155/2022/5953561

[12] Fouda, A.E.S., El-Dossoki, F.I., Atia, M.F., Abd El Aziz, F.M. and El-Hossiany, A. (2025) Contribution to the Corrosion Inhibition of Aluminum by Aqueous Extract

of *Moringa oleifera* in 2 M HCL. *Discover Chemical Engineering*, **5**, Article No. 1. https://doi.org/10.1007/s43938-025-00074-z

[13] Manh, T.D., Huynh, T.L., Thi, B.V., Lee, S., Yi, J. and Nguyen Dang, N. (2022) Corrosion Inhibition of Mild Steel in Hydrochloric Acid Environments Containing *Sonneratia caseolaris* Leaf Extract. *ACS Omega*, **7**, 8874-8886. https://doi.org/10.1021/acsomega.1c07237

[14] Mamudu, U., Santos, J.H., Umoren, S.A., Alnarabiji, M.S. and Lim, R.C. (2024) Investigations of Corrosion Inhibition of Ethanolic Extract of *Dillenia suffruticosa* Leaves as a Green Corrosion Inhibitor of Mild Steel in Hydrochloric Acid Medium. *Corrosion Communications*, **15**, 52-62. https://doi.org/10.1016/j.corcom.2023.10.005

[15] Jeetendra, B. and Pramod, J. (2022) Corrosion Inhibition Potential of *Mentha spicata* Extract on Mild Steel in Acidic Medium. *Iranian Journal of Chemistry and Chemical Engineering*, **41**, 3365-3376.

[16] Alimohammadi, M., Ghaderi, M., *et al.* (2023) *Falcaria vulgaris* Leaves Extract as an Eco-Friendly Corrosion Inhibitor for Mild Steel in Hydrochloric Acid Media. *Scientific Reports*, **13**, Article No. 3737. https://doi.org/10.1038/s41598-023-30571-6

[17] Velázquez-González, M.A., Gonzalez-Rodriguez, J.G., Valladares-Cisneros, M.G. and Hermoso-Diaz, I.A. (2014) Use of *Rosmarinus officinalis* as Green Corrosion Inhibitor for Carbon Steel in Acid Medium. *American Journal of Analytical Chemistry*, **5**, 55-64. https://doi.org/10.4236/ajac.2014.52009

[18] Majd, M.T., Asaldoust, S., Bahlakeh, G., Ramezanzadeh, B. and Ramezanzadeh, M. (2019) Green Method of Carbon Steel Effective Corrosion Mitigation in 1 M HCL Medium Protected by *Primula vulgaris* Flower Aqueous Extract via Experimental, Atomic-Level MC/MD Simulation and Electronic-Level DFT Theoretical Elucidation. *Journal of Molecular Liquids*, **284**, 658-674. https://doi.org/10.1016/j.molliq.2019.04.037

[19] Kaushik, N.P., Rao, P., Kedimar, N. and Rao, S.A. (2024) Grape Seed Extract as an Environment-Friendly Green Inhibitor for Corrosion of Mild Steel in 1 M Sulfamic Acid. *Journal of Materials Engineering and Performance*, **33**, 10885-10894. https://doi.org/10.1007/s11665-024-09802-y

[20] Fouda, A.E.-A.S., Etaiw, S.E.d.H., Bakr, M.M. and Shalabi, K. (2021) Ashwagandha Extract as Green Sustainable Corrosion Inhibitor for Aluminum in Acidic Solutions. *Biointerface Research in Applied Chemistry*, **11**, 9719-9734. https://doi.org/10.33263/BRIAC112.97199734

[21] Meena, O., Kaushal, S., Kumar, S. and Dalal, J. (2024) *Euphorbia neriifolia* Extracts as Green Corrosion Inhibitors for Aluminium in Hydrochloric and Nitric Acid Media. *Discover Materials*, **4**, Article No. 102. https://doi.org/10.1007/s43939-024-00157-8

[22] Barghout, N.A., El Nemr, A., Abd-El-Nabey, B.A., Fetouh, H.A., Ragab, S. and Eddy, N.O. (2022) Use of Orange Peel Extract as an Inhibitor of Stainless Steel Corrosion during Acid Washing in a Multistage Flash Desalination Plant. *Journal of Applied Electrochemistry*, **53**, 379-399. https://doi.org/10.1007/s10800-022-01772-0

[23] Fattah-Alhosseini, A., Karbasi, M., Chaharmahali, R., Fardosi, A. and Kaseem, M. (2024) An Overview of Electrochemical, Non-Electrochemical and Analytical Approaches for Studying Corrosion in Magnesium and Its Alloys. *Journal of Magnesium and Alloys*, **12**, 3516-3542. https://doi.org/10.1016/j.jma.2024.08.017

[24] Malaret, F. (2022) Exact Calculation of Corrosion Rates by the Weight-Loss Method.

Experimental Results, **3**, e13. https://doi.org/10.1017/exp.2022.5

[25] Akbas, E., Ruzgar, A., Akbas, C. and Sahin, E. (2022) Synthesis, Characterization, and DFT Calculation of Some New Pyrimidine Derivatives and Theoretical Studies on the Corrosion Inhibition Performance. *Iranian Journal of Chemistry and Chemical Engineering*, **41**, 1643-1656.

[26] Diki, N.Y.S., Coulibaly, N.H., Kambiré, O. and Trokourey, A. (2021) Experimental and Theoretical Investigations on Copper Corrosion Inhibition by Cefixime Drug in 1M HNO_3 Solution. *Journal of Materials Science and Chemical Engineering*, **9**, 11-28. https://doi.org/10.4236/msce.2021.95002

[27] Ogunyemi, B.T., Latona, D.F., Ayinde, A.A. and Adejoro, I.A. (2020) Theoretical Investigation to Corrosion Inhibition Efficiency of Some Chloroquine Derivatives Using Density Functional Theory. *Advanced Journal of Chemistry-Section A*, **3**, 485-492. https://doi.org/10.33945/sami/ajca.2020.4.10

[28] Mahgoub, F.M. and Al-Rashdi, S.M. (2016) Investigate the Corrosion Inhibition of Mild Steel in Sulfuric Acid Solution by Thiosemicarbazide. *Open Journal of Physical Chemistry*, **6**, 54-66. https://doi.org/10.4236/ojpc.2016.63006

[29] Mamudu, U., Alnarabiji, M.S. and Lim, R.C. (2023) Adsorption Isotherm and Molecular Modeling of Phytoconstituents from *Dillenia suffruticosa* Leaves for Corrosion Inhibition of Mild Steel in 1.0 M Hydrochloric Acid Solution. *Results in Surfaces and Interfaces*, **13**, Article 100145. https://doi.org/10.1016/j.rsurfi.2023.100145

[30] Koffi, A.A., Coulibaly, S., Yeo, M., Coulibaly, K.K. and Niamien, P.M. (2025) Delving Ethyl 2-Oxo-2H-Chromene-3-Carboxylate as a Corrosion Inhibitor for Aluminum in Acidic Environments. *Oriental Journal of Chemistry*, **41**, 57-65. https://doi.org/10.13005/ojc/410106

[31] Minjibir, S.A. and Ladan, M. (2023) Corrosion Inhibition Potential of *Prosopis juliflora* Leaves Extract on Mild Steel in H_2SO_4 Solutions. *Advanced Journal of Chemistry, Section A*, **6**, 311-323.

[32] Mu'azu, I., Ayuba, A.M., Hussein, M. and Fater, I. (2024) Corrosion Inhibition of Mild Steel in 0.3 M Hydrochloric Acid Solution Using *Urena lobata* Leaves Extract. *Applied Journal of Environmental Engineering Science*, **10**, 206-223.

[33] Muthamma, K., Kumari, P., Lavanya, M. and Rao, S.A. (2021) Corrosion Inhibition of Mild Steel in Acidic Media by N-[(3,4-Dimethoxyphenyl)Methyleneamino]-4-Hydroxy-Benzamide. *Journal of Bio- and Tribo-Corrosion*, **7**, 1-19. https://doi.org/10.1007/s40735-020-00439-7

[34] Kedimar, N., Rao, P. and Rao, S.A. (2023) Effect of Ionic Liquid as Corrosion Inhibitor for 6061 Aluminium Alloy-(*Electrochemical and Quantum Chemical Approaches*). *Materials Technology*, **38**, 1-16. https://doi.org/10.1080/10667857.2023.2238414

[35] Bader, A., Shaheen, U., Aborehab, M.A.S., El Ouadi, Y., Bouyanzer, A., Hammouti, B., *et al.* (2018) Inhibitory Effect of *Acacia hamulosa* Methanolic Extract on the Corrosion of Mild Steel in 1 M Hydrochloric Acid. *Bulletin of the Chemical Society of Ethiopia*, **32**, 323-335. https://doi.org/10.4314/bcse.v32i2.11

[36] EL-Haddad, M.N. and Fouda, A.S. (2025) Investigating *Xanthium spinosum* Extract as an Eco-Friendly Corrosion Inhibitor for Aluminium in Acidic Environments: A Green Approach to Metal Protection. *Results in Chemistry*, **14**, Article 102136. https://doi.org/10.1016/j.rechem.2025.102136

[37] Méndez, C.M., Gervasi, C.A., Pozzi, G. and Ares, A.E. (2023) Corrosion Inhibition of Aluminum in Acidic Solution by *Ilex paraguariensis* (*Yerba mate*) Extract as a Green Inhibitor. *Coatings*, **13**, Article 434. https://doi.org/10.3390/coatings13020434

[38] Minagalavar, R.L., Rajappa, S.K., Rathod, M.R., Sajjan, A.M. and Sujatha, K. (2025)

Investigation of Corrosion Inhibition of Low Carbon Steel Using Expired Drug Levocetirizine as a Potential Corrosion Inhibitor in 0.5 M H_2SO_4 Medium. *Discover Electrochemistry*, **2**, Article No. 4. https://doi.org/10.1007/s44373-025-00018-w

[39] Chadili, M., Rguiti, M.M., El Ibrahimi, B., Oukhrib, R., Jmiai, A., Beelkhaouda, M., *et al.* (2021) Corrosion Inhibition of 3003 Aluminum Alloy in Molar Hydrochloric Acid Solution by Olive Oil Mill Liquid By-Product. *International Journal of Corrosion*, **2021**, Article ID: 6662395. https://doi.org/10.1155/2021/6662395

[40] Lakbaibi, Z., Damej, M., Molhi, A., Benmessaoud, M., Tighadouini, S., Jaafar, A., *et al.* (2022) Evaluation of Inhibitive Corrosion Potential of Symmetrical Hydrazine Derivatives Containing Nitrophenyl Moiety in 1M HCL for C38 Steel: Experimental and Theoretical Studies. *Heliyon*, **8**, e09087. https://doi.org/10.1016/j.heliyon.2022.e09087

[41] Wahba, A.M., Shoueir, K. and Fouda, A.E.S. (2025) Prediction and Evaluation of Pyrimidinones Derivatives: DFT Analysis, Corrosion Inhibition, and Bioactivity Studies. *Results in Surfaces and Interfaces*, **18**, Article 100448. https://doi.org/10.1016/j.rsurfi.2025.100448

[42] Boughazi, H., Boudinar, Y., Tlili, S., Djedouani, A. and Naili, N. (2025) Electrochemical, Surface, DFT, and ADMET Insights into (*e*)-2-(2-Hydroxybenzylidene)Hydrazine-1-Carboxamide as a Corrosion Inhibitor. *RSC Advances*, **15**, 38946-38968. https://doi.org/10.1039/d5ra05876g

[43] Oyeneyin, O.E., Ojo, N.D., Ipinloju, N., Agbaffa, E.B. and Emmanuel, A.V. (2022) Investigation of the Corrosion Inhibition Potentials of Some 2-(4-(Substituted)Arylidene)-1H-Indene-1,3-Dione Derivatives: Density Functional Theory and Molecular Dynamics Simulation. *Beni-Suef University Journal of Basic and Applied Sciences*, **11**, 1-14. https://doi.org/10.1186/s43088-022-00313-0

[44] Ayuba, A.M., Iorhuna, F. and Nyijime, A.T. (2024) Corrosion Inhibition Activities of Acridine Derivatives on Aluminium Using Fukui Function and Molecular Dynamic. *Progress in Chemical and Biochemical Research*, **7**, 453-471.

[45] Ibrahim, M.A.A., Moussa, N.A.M., Mahmoud, A.H.M., Sayed, S.R.M., Sidhom, P.A., Abd El-Rahman, M.K., *et al.* (2023) Density Functional Theory Study of the Corrosion Inhibition Performance of 6-Mercaptopurine and 6-Thioguanine Expired Drugs toward the Aluminium (111) Surface. *RSC Advances*, **13**, 29023-29034. https://doi.org/10.1039/d3ra04954j

[46] Bine, F.K., Tasheh, S.N. and Nkungli, N.K. (2021) Corrosion Inhibition of Aluminium in Gas and Acid Media by Some Chalcone-Based N-(3-Aminopropyl)Imidazoles: TD-DFT-Based FMO, Conceptual DFT, QTAIM and EDA Studies. *Computational Chemistry*, **9**, 37-63. https://doi.org/10.4236/cc.2021.91003